IEEE Access
Multidisciplinary | Rapid Review | Open Access Journal

Received August 31, 2021, accepted September 10, 2021, date of publication September 24, 2021, date of current version October 4, 2021.

Digital Object Identifier 10.1109/ACCESS.2021.3115595

Development of an Unmanned Aerial System for Maritime Environmental Observation

SUNGHUN JUNG[1], (Member IEEE), AND WONKOOK KIM[2], (Member, IEEE)
[1]Faculty of Smart Vehicle System Engineering, Chosun University, Dong-gu, Gwangju 80305, South Korea
[2]Department of Civil and Environmental Engineering, Pusan National University, Geumjeong-gu, Busan 43241, South Korea

Corresponding author: Wonkook Kim (wonkook@pusan.ac.kr)

This work was supported by a research fund from Chosun University, 2020, under Grant K208419002.

ABSTRACT We developed an octocopter-based unmanned aerial system (UAS) to monitor remote environments. The system contains various environmental monitoring sensors for measuring wind speed/direction, temperature, relative humidity, atmospheric pressure, fine dust, and multispectral and RGB data. The UAS consists of an unmanned aerial vehicle (UAV), a ground control station, and a server. We studied its electrical, mechanical, and software (SW) configurations. Specifically, we developed hardware (HW) and SW to control the yaw and gimbal pitch directions of the UAV conveying multispectral and RGB cameras. To prevent the obtained solar reflectance from affecting the multispectral and RGB data and to improve the quality of the obtained data, we maneuvered the yaw so that it would always deviate 135° from the solar azimuth angle, with the sun at its rear. Managing the yaw direction involves controlling the UAV based on a micro air vehicle link message-based robot operating system (ROS). To safely test the UAS performance before the maiden flight in an ocean area, we first evaluated PX4 and ROS-based SW through indoor software-in-the-loop simulation (SILS) via the Gazebo tool. Subsequently, we used an F450 UAV and an actual maritime UAV to sequentially perform pre-flight and flight experiments. This paper explains the system operation scenario, UAS component, and simulation and experimental results. The results reveal that the average yaw angle error during the mission, $\left|\theta_{y,des} - \theta_y\right|$, is approximately 8°, and the average pitch angle of the gimbal during the mission, $\left|50° - \left|\bar{\theta_c}\right|\right|$, is less than 5°.

INDEX TERMS Maritime environmental observation, ocean color, robot operating system, unmanned aerial system, unmanned aerial vehicle.

I. INTRODUCTION

Satellites [1], [2], crewed aircraft [3], [4], and vessels [5] generally capture ocean color, which is a critical indicator of ocean conditions. However, obtaining images of desired locations at desired times may be difficult when using conventional remote sensing based on satellites, airplanes, and vessels owing to the inaccessibility of certain regions and inclement weather. Consequently, it may be challenging to capture anomalies, such as a red tide in the ocean [6], which requires immediate or time-based observations. Understanding phenomena such as the resuspension–precipitation process of suspended solids and the spread of low-salinity water originating in coastal areas is also difficult.

To measure the remote-sensing reflectance (Rrs) of seawater and estimate its constituents (such as phytoplankton chlorophyll concentration and marine inherent optical properties), researchers have widely used AWRs, either by transporting portable AWRs on a ship or by installing them at fixed observation points. Herein, we define Rrs as the water-leaving (Lw) radiance, normalized by the downwelling irradiance (Ed), and we measure both Lw and Ed above the sea surface. However, the use of the aforementioned method to measure the remote reflectance in various seawater environments multiple times is expensive. Furthermore, measuring it at the desired frequency in the desired sea area at the expected time is impossible during inclement weather. In addition, it is advantageous to monitor anomalies with continuous observation data for stationary observations. However, data from various sea areas cannot be obtained because the observation data are limited to stationary data.

Nevertheless, we can instantly capture various marine phenomena by using an unmanned aerial system (UAS), including vertical takeoff and landing (VTOL)-type unmanned

The associate editor coordinating the review of this manuscript and approving it for publication was Stefania Bonafoni.

aerial vehicles (UAVs). UAVs can move and hover over a location and obtain high-resolution data of the desired form in real-time. Specifically, using a micro-sized multi-copter UAV can measure real-time data for distances up to tens of kilometers, allowing sufficient monitoring of anomalies that occur near coastal areas or moving ships in the middle of a vast sea [7]–[9]. Because of the above-mentioned benefits, UAS can be used for marine fauna surveys in place of crewed aircraft [10]–[18].

II. RELATED WORK

For robust automatic UAS operation in a maritime environment subject to frequent gusts and strong winds, where a single mistake could result in catastrophic system destruction (due to ocean salinity) or loss into the sea, cutting-edge system development and data analysis techniques are essential to:

- Develop an error-free and fully automatic UAS.
- Maneuver the unmanned system to maintain the desired attitude from any possible internal or external erroneous source.
- Accomplish the environmental data acquisition mission without losing or damaging the incoming data.
- Induce processed data that are as accurate as the direct measurement data.

We performed a literature survey on the following four general topics related to the UAS for maritime environmental observations:

- Automatic system development.
- Attitude-control algorithm development, considering the solar location.
- Data measurement and analysis.
- Latest technology.

A. AUTOMATIC UAS DEVELOPMENT

The fully automatic mission operation of the UAS requires system development, which can be divided into three main categories: software (SW), hardware (HW), and system integration.

- SW development involves the PX4 open-source FC SW platform and the Gazebo SW simulator-based obstacle avoidance flight operation [19].
- Ebeid *et al.* thoroughly surveyed and summarized HW development, one of the most important parts of a UAV that involves an open-source platform-based and commercially available flight controller (FC) [20]. Jackson *et al.* developed and analyzed a low-cost and lightweight embedded FC, incorporating a robot operating system (ROS) on a Linux computer (called ROSflight), with respect to loop rate, communication bandwidth, and flight experiments [21].
- System integration involves a vision-guided UAV for the automatic landing mission using an in-house developed FC and avionics hub board, gimbal, camera, laser rangefinder, MC, and wireless module [22].

B. UAV ATTITUDE-CONTROL ALGORITHM

To obtain environmental data from the desired location and position, the attitude of the UAV must be maneuvered as quickly and precisely as possible.

- Haus *et al.* presented and applied the centroid vectoring technique-based attitude-control method — which uses the concept of a robot dynamic model and ubiquitous Jacobian matrix — to both aerial and underwater vehicles [23].
- Segales *et al.* combined a stability augmentation system (SAS) and a control augmentation system (CAS), which are PID controller-based, to maneuver the attitude of the tricopter UAV [24].

C. SOLAR-TRACKING ALGORITHM

Specifically, to achieve efficient optical and multispectral data of the sea surface, the sensor direction must be controlled by referring to the solar location so that the amount of sunlight on the obtained optical and multispectral data is minimized. For this purpose, a solar-tracking algorithm should be considered along with the UAV attitude-control algorithm.

- Calculating the solar location and building a low-cost solar-tracking mechanism involves solar-tracking mathematical models, along with active and chronological algorithms 25].
- Developing a low-cost closed-loop solar-tracking system involves using the solar-positioning algorithm to estimate solar azimuth and elevation angles, which is eventually used to position the solar panel toward the sun [26].
- Jamroen *et al.* developed a pseudo-azimuthal system model for calculating the solar altitude and azimuth angles for a solar tracking system [27].

D. MARITIME ENVIRONMENTAL DATA MEASUREMENT

Numerous studies have used UAVs and unmanned surface vehicles (USVs) to obtain maritime environmental data.

- O'Young and Hubbard conducted a maritime surveillance project using a small fixed-wing UAV for a detailed analysis of several categories, including maritime surveillance, beyond-line-of-sight control, and human factors [28].
- To investigate aquatic environmental pollution, Zang *et al.* developed a fixed-wing UAV with a modified catapult launching system, parachute landing system, and a high-powered engine [29].
- Cook *et al.* used an autonomous fixed-wing UAV to collected meteorological data, including air temperature and relative humidity (RH) for coastal atmospheric research applications, at heights of up to 500 m and distances of up to 25 km [30].
- Several researchers have developed a relatively low-cost small USV [31], [32] and an amphibious vehicle [33] with the functions of both UAV and USV to monitor the quality of rivers or reservoirs based on pH, dissolved

oxygen, turbidity, electrical conductivity, temperature, and chlorophyll-a.
- For studying the morphodynamic states of beach topology, Casella *et al.* used a UAV to generate digital elevation models of the beach [34].
- Sorensen *et al.* developed a low-cost and open-source SW-based small UAV equipped with a mechanism that provides easily interchangeable measurement sensors and tested it in a lake [35].

E. MARITIME ENVIRONMENTAL DATA ANALYSIS

Unmanned system development been researched for safe, rapid, and low-cost (but robust) data collection; active maritime data analysis research is also in progress to overcome the limitations of remote data.
- The characteristics of a coastal environment based on both coastline change and marine litter concentration in shoreline zones have been determined using a UAS based on the geoinformation produced using the UAS-structure from motion (UAV-SfM) pipeline method [36].
- The Rrs of seawater is the most fundamental optical property for remotely estimating components in seawater, including chlorophyll concentration, suspended solid concentration, and colored dissolved organic matter. To estimate seawater components and phenomena from Rrs, it is necessary to develop algorithms using the accumulated seawater reflectivity and constituent data under various seawater and atmospheric conditions, as discussed in a previous work [37].
- A method incorporating both superpixel segmentation and a convolutional neural network (CNN) was proposed for extracting accurate *Ulva prolifera* (a green seaweed species) region from superpixel UAV image classification [38].
- The UAS has been used to detect marine litter, such as floating plastics [39], [40].
- The methodology and practical information of UAV-based photography for oceanographers to lower barriers to entry reduced the cost of developing robust unmanned systems and obtained high-quality and map-ready data [41].
- A protocol to enhance the reliability of environmental data acquisition using UAVs is presented by considering the morphology, environmental conditions, and flight parameters 42].
- For satellite image classification, high-resolution images observed by a UAV with a resolution below 5 cm were used for support vector machine data training [43].

F. LITERATURE REVIEW

Several studies have reviewed various applications of UASs for environmental monitoring [44]–[46]. Specifically, these reviews dealt with environmental data measurement; processing; assessment; and limitations of the land, air, and sea; as well as maritime archeology, pollutants, physical and biological oceanography, wildlife, behavioral ecology, habitat assessments, coastal geomorphology, etc.

G. MAIN CONTRIBUTION

The novelty of our study is the development and verification of real-time data broadcasting UAS to retrieve three-dimensional (3D) maritime environmental observation data by reducing the reflected light with automatic UAV yaw and gimbal pitch angle control.

In this study, we primarily focused on developing an environmentally monitored UAS. Specifically, we designed the UAV to automatically control both the pitch and yaw directions of multispectral and RGB cameras, based on the solar incident angle, to calculate the reflected light shown on the captured image and eliminate sunglint. Simultaneously, to remotely estimate the seawater constituents by calculating the reflected light from the surface of the sea, we needed to install a multispectral sensor with a gimbal to obtain two-directional data (obtained at an inclination of 40° from the top and bottom) [47]. Furthermore, to construct a 3D environmental map, we developed a UAV to obtain additional data, including wind speed/direction, temperature, RH, atmospheric pressure, fine dust, multispectral, and RGB data. Finally, we synchronized the data in real-time using a server located in a remote area through long-term evolution (LTE) and Wi-Fi communication.

The rest of this paper is organized as follows:
- Section III describes the system design of the UAS operation.
- Sections IV, V, and VI present overviews of the electrical system, mechanical system, and SW configurations of the UAV, ground control station (GCS), and server.
- Section VII details the indoor and outdoor flight experiments with the corresponding flight logs and their analyses.
- Section VIII presents 3D environmental maps generated from data obtained from outdoor flight experiments.
- Section IX presents our conclusions and directions for future work.

III. SYSTEM DESIGN

A. SYSTEM REQUIREMENTS

For non-professional use in maritime environmental observation, we needed to develop a UAS that incorporates a low-altitude VTOL-capable UAV that:
- Can be produced and repaired at a relatively low cost.
- Is fully automatic and does not require any human intervention during mission flight.
- Can be operated only under the line of sight.
- Can be easily transported and deployed by one operator during the entire mission.
- Can synchronize sensor measurement data from the UAV to the server through real-time LTE.
- Can control the UAV yaw angle based on the solar azimuth angle to minimize sun glint.

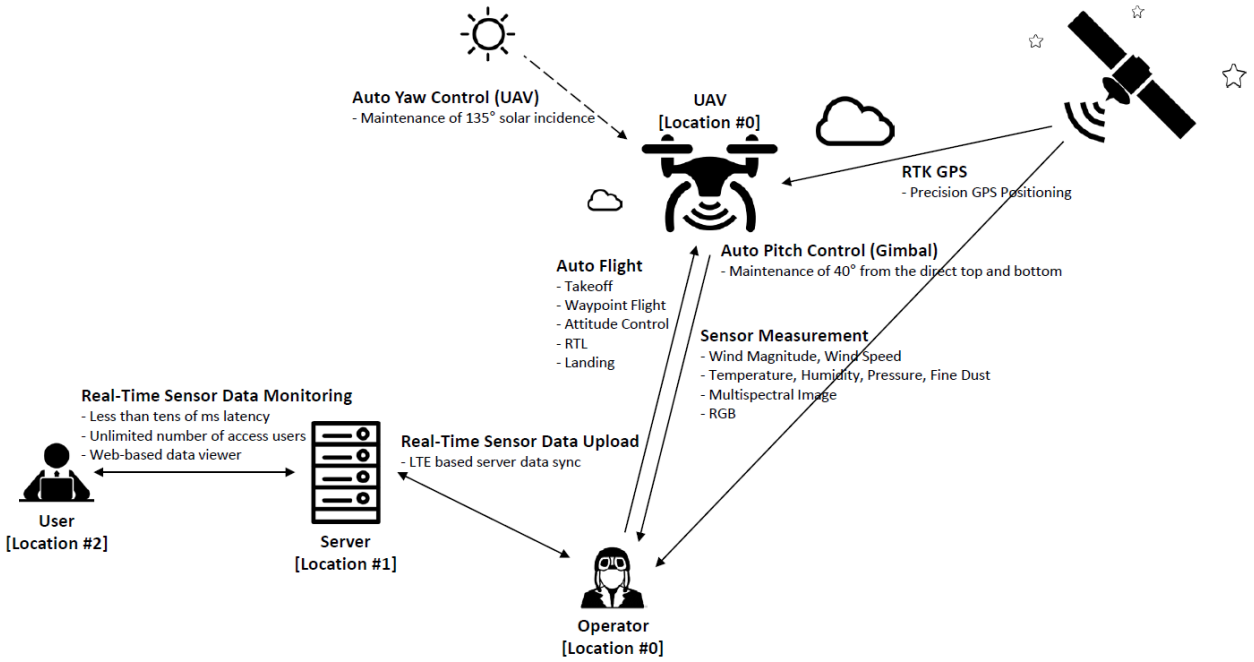

FIGURE 1. Overview of UAS operation for environmental observation.

- Can control the gimbal pitch angle to capture both ocean and sky images using both multispectral and RGB cameras.
- Can be operated only under the altitude of several hundred meters.
- Runs an open-source PX4 autopilot as an FC.
- Runs Ubuntu and a robot operating system (ROS) on a mission computer (MC).

B. OPERATION OVERVIEW

For automatic 3D data acquisition using a UAV, Figs. 1 and 2 provide an overview of the UAS operation and an operational scenario. Several mandatory restrictions must be considered.

- The UAV starts its operations from a stationary ship (moving slowly over time) or on the ground.
- The UAV is at an altitude of 30 m and backs the sun at approximately 135°, and the camera headed at 40° from the bottom rotates to a heading angle of 40° from the top over a pre-assigned period [48]. The attitude of the UAV — specifically, the yaw angle — should be calculated based on the solar position from the global positioning system (GPS) location and current time.
- After the mission operation, the UAV should return to the launch location, which may be different from the original position.
- All mission operations must be controlled using a user-friendly graphical user interface (GUI) to enable use by non-experts.
- The UAV should not only perform basic operations, including circular flight, ascending, descending, and flying to a specific location and hovering during mission operations but also all functions provided by the QGroundControl (QGC) software [49].

In Fig. 2, the yellow lines represent the path of the UAV, and the green lines represent the path of the image center of both the multispectral camera and RGB camera. The red marks along the yellow path represent the waypoints of the UAV.

C. OPERATION MANUAL

For non-expert use, we minimized and fully automated the UAS operation processes, as presented in the UAS operation manual in Table 1. In total, the UAS required seven steps, including connecting the operator's smartphone LTE communication with the GCS to disarm the UAV motors after mission completion.

TABLE 1. UAS Operation Manual.

Step	Detail
1	Establish LTE communication by connecting the GCS and a smartphone.
2	Connect battery packs to the UAV and wait until the start beep ceases and the gimbal levels.
3	Use GCS to open a terminal in the Ubuntu operating system (OS) and run the ./run.sh bash script to execute QGC, GCS GUI, sensor data acquisition code, and roscore.
4	Use QGC to insert the desired waypoints for sensor data measurements.
5	Click the *Start* button located next to *Mission* to launch the UAV mission flight.
6	Click the *Hold* button located next to *Mission* to make the UAV hover.
7	Click the *End* button located next to *Mission* to end the mission during the flight. Even if the *End* button is not clicked, the UAV automatically returns to its home position, lands, and disarms the motors after mission completion.

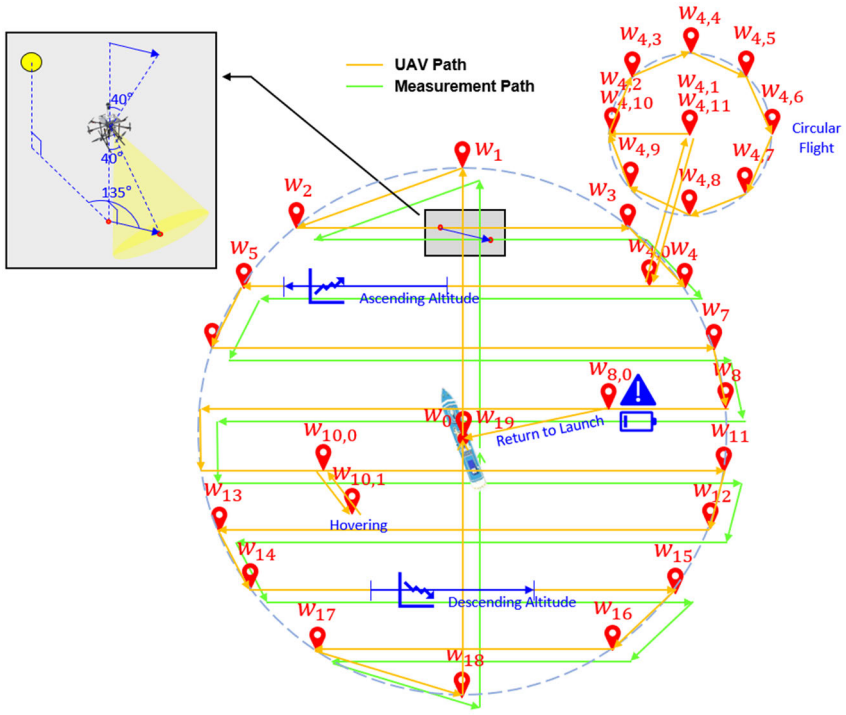

FIGURE 2. UAV operation scenario.

D. OPERATION STEPS

To commence the UAS operation, we placed the UAV on the ground, as shown in Fig. 3(a), and then installed two tripods, one for Here+ real-time kinematic (RTK) GPS and another for Ubiquity Nanostation NSM5, as shown in Fig. 3(b). For safety purposes, we placed the UAV at a sufficient distance from the GCS operator. As soon as we performed a thorough system check, the operator started the mission and we removed the UAV, as shown in Fig. 3(b). During the mission, the operator monitored incoming data from both the UAV and sensors for emergencies, as shown in Figs. 3(c) – (e). Fig. 3(f) shows that after the UAV reached the final waypoint, it automatically returned to the home position, landed, and turned off all motors.

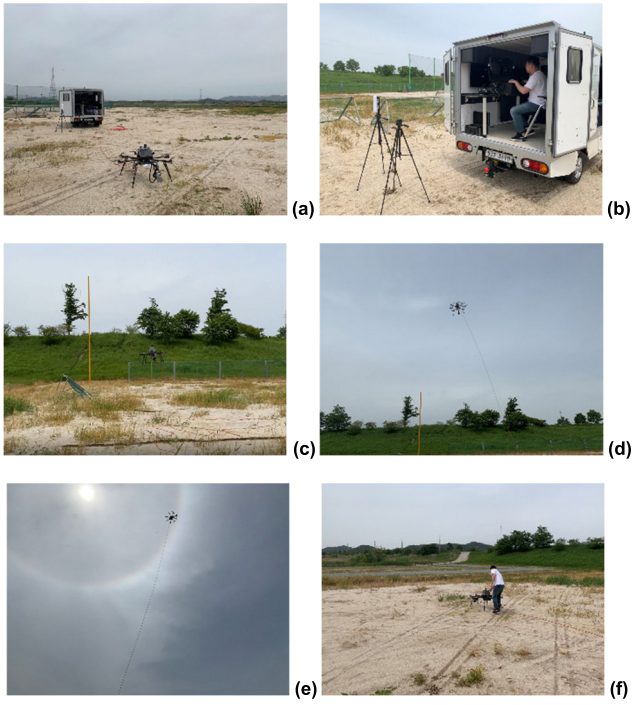

FIGURE 3. Step-by-step procedure, from preparing UAS to retrieving the UAV.

E. SOFTWARE CONFIGURATION

The total SW architecture consists of the UAV, operator, server, and user, as shown in Fig. 4, from right to left.

- The UAV SW part comprises environmental sensor operation codes (ft742.py, rededge.py, ocam.py, pth200.py, and sds011.py), environmental sensor data files (ft742.txt, rededge_xxx.png, ocam_xxx.png, pth200.txt, and sds011.txt), and a gimbal operation code (gremsy.cpp).
- The software operator comprises an overall system operation code (run.sh), operator GUI operation code (gui.py), solar incidence calculation code (solar.py), UAV operation code (catkin_ws-related files qgc.py, and roscore.py), environmental sensor synchronization code (remotedata.py), and environmental sensor data files (ft742.txt, rededge_xxx.png, ocam_xxx.png, pth200.txt, and sds011.txt).
- The server SW part comprises environmental sensor data files (ft742.txt, rededge_xxx.png, ocam_xxx.png,

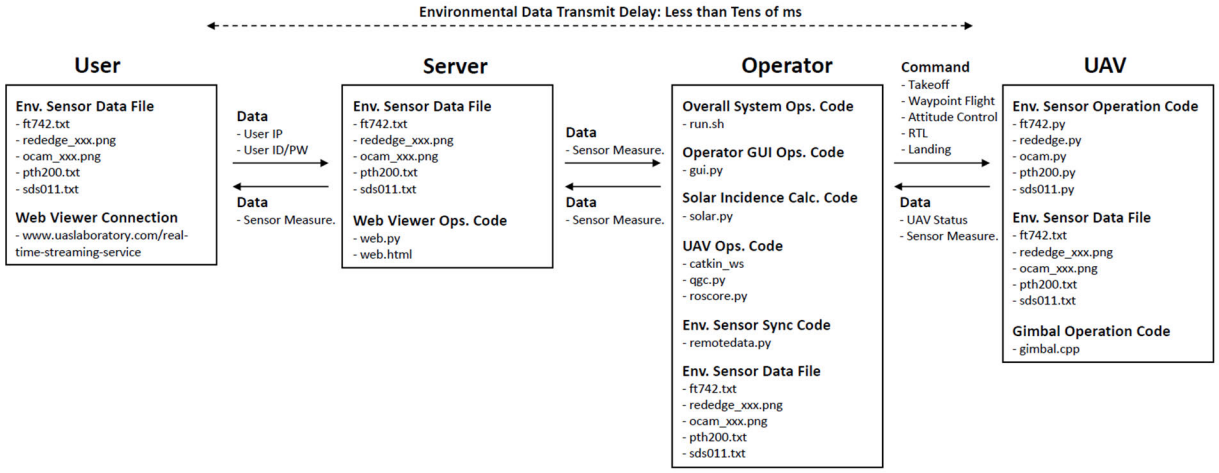

FIGURE 4. Conceptual diagram of UAS operation for environmental observation.

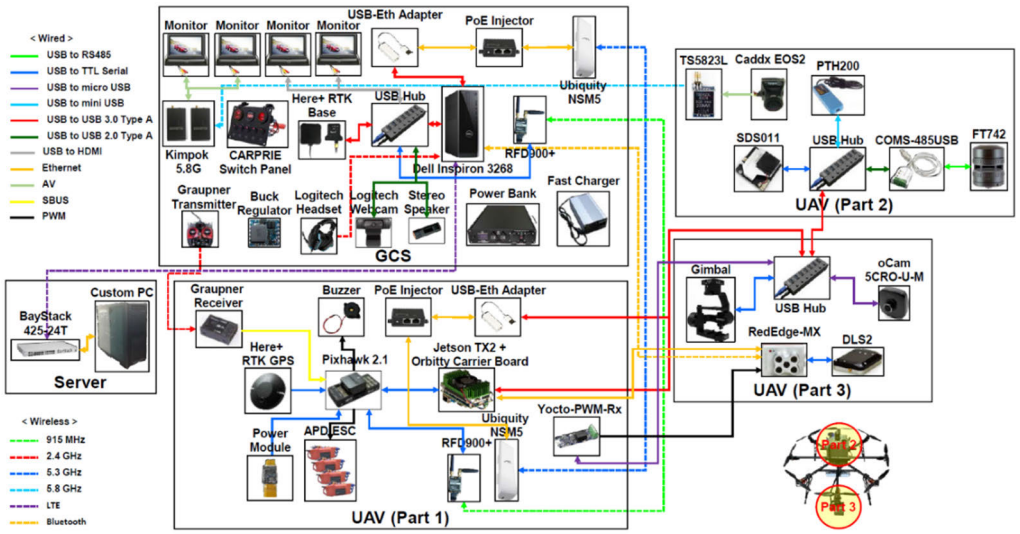

FIGURE 5. Communication configuration of UAS.

pth200.txt, and sds011.txt) and web viewer operation code (web.py and web.html).

- The user SW part comprises the environmental sensor data file (ft742.txt, rededge_xxx.png, ocam_xxx.png, pth200.txt, and sds011.txt). Users can connect via a website to check the incoming environmental data from the UAV in real-time.

F. COMMUNICATION CONFIGURATION

Fig. 5 shows the wired and wireless communication configurations of the GCS, UAV, and server. Specifically, the communication configuration of the UAV comprises three sub-parts: the UAV communication configuration, the communication configuration of the sensors located on the central hub of the UAV, and the communication configuration of the sensors mounted on the gimbal mounted under the motor in the heading direction.

G. MEASUREMENT PROTOCOL

Table 2 lists the UAV and sensor data necessary for systematic data management. Although a slight time difference occurs between the data measured by each sensor, the data transmission rate was sufficiently low to prevent data transmission loss.

H. MATHEMATICAL APPROACH

Because the UAV heading angle was 135° from the sun and the gimbal attached to the end of the heading arm was tilted 40° from the bottom, we preplanned the route of the UAV so that the field of view (FOV) of the camera attached to the gimbal covered the region of interest (ROI), as shown in Fig. 6. Here, the positive x-axis and y-axis represent the north and west directions, respectively.

For simplicity, we assumed that the center of the FOV (P_f) should go over the polygon corners (S_i), which were selected

TABLE 2. Data Protocol of Sensor Measurement.

		Type	Unit	Values
Data Number		Int	-	min: 0, increment: 1
Date Time	Date	Int	s	min: 0, increment: 1
	Time	Int	s	min: 0, increment: 1
Global Position	Lon	Int	deg	-
	Lat	Int	deg	-
	Alt	Int	m	min: 0, increment: 1
UAV	Roll	Float	rad	min: −pi, max: +pi
	Pitch	Float	rad	min: −pi, max: +pi
	Yaw	Float	rad	min: −pi, max: +pi
	Desired Yaw	Float	rad	min: −pi, max: +pi
Solar Azimuth		Int	deg	min: 0, max: +360, increment: 1
Gimbal Pitch		Float	rad	min: −pi/2, max: +pi/2
Wind	Speed	Float	m/s	min: 0, increment: 0.1
	Direction	Int	deg	min: 0, max: +360, increment: 1
Temperature		Float	°C	min: −40, max: +70, increment: 0.01
RH		Float	%	min: 0, max: +360, increment: 1
Atmospheric Pressure		Float	kPa	min: 0, max: +120, increment: 0.01
Particle Matter (PM)	2.5	Float	μg/m^3	min: 0, max: +999, increment: 1
	10	Float	μg/m^3	min: 0, max: +999, increment: 1
Image	Multispectral	Bool	-	min: false, max: true
	RGB	Bool	-	min: false, max: true

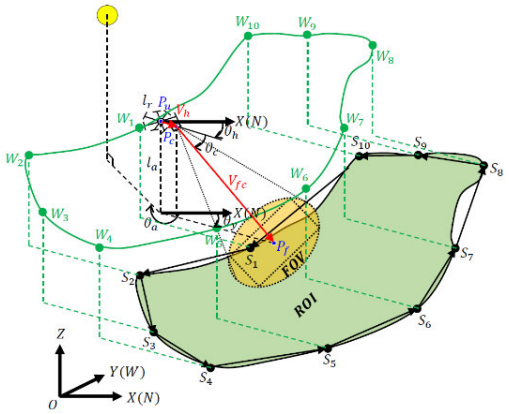

FIGURE 6. Path planning of the UAV.

points on the ROI; i.e., the P_f should be located inside the polygon drawn by the selected points, S_i.

Based on this, we can calculate the desired waypoints (W_i) for use as a list of input waypoints in the QGC SW, as follows:

$$P_{u,i} = S_i - R_y(\theta_h)\, V_{fc}^T - R_z\left(\frac{\pi}{2} - \theta_c\right) V_h^T = W_i \quad (1)$$

where $P_{u,i}$ is the UAV position, i.e., $[(x, y, z)_u$ and $i = 1, 2, \ldots, n]$, which is in agreement with the desired waypoints (W_i); $R_y(\theta_h)$, is the rotation matrix of θ_h around the y-axis; θ_h is the heading angle of the UAV ($\theta_h = \theta_a \pm \frac{135° \cdot \pi}{180°}$), which is the same as the yaw angle of the UAV (θ_y); θ_a is the solar azimuth angle; V_{fc} is the vector pointing to the center of the camera frame from the gimbal ($|V_{fc}| = \frac{l_a}{\cos\theta_c}$); l_a is the UAV altitude; $R_z(\theta_c)$ is the rotation matrix of θ_c around the z-axis; θ_c is the angle measured from the XY plane to V_{fc} ($\theta_c = \frac{40° \cdot \pi}{180°}$), which is the same as the pitch angle of the gimbal; V_h is the vector pointing to the end of the heading arm from the center of the UAV ($|V_h| = l_r$); l_r is the length of the UAV arm; and P_c represents the camera position $[x, y, zc]$.

IV. UNMANNED AERIAL VEHICLE

A. SYSTEM REQUIREMENTS

The UAV needed to transport various environmental sensors; specifically, a gimbal carrying a multispectral camera and an RGB camera, which were installed such that they would face the same direction. In addition, the UAV needed to refer to the predefined waypoints as it flowed over the mission area.

The main functions of the UAV can be summarized as follows:

- The flight operation commands, such as takeoff, waypoint flight, attitude control, return to launch (RTL), and landing.
- The yaw angle that the UAV had to head to and maintain a 135° bearing from the solar azimuth angle, with the sun at its rear.
- The pitch angle of the gimbal was maintained to allow both a multispectral camera and an RGB camera inclined at an angle of 40° from the exact vertical, which periodically changes its bearing to 40° from the top to 40° from the bottom, as shown in Fig. 7.
- Carry environmental sensors to collect data and send them to the GCS.

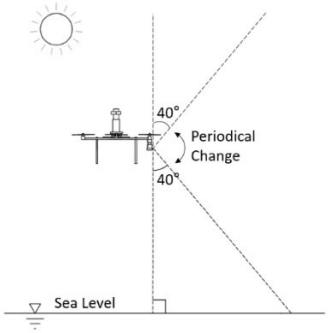

FIGURE 7. Conceptual description of pitch angle control of gimbal mounted on UAV.

B. ELECTRICAL SYSTEM CONFIGURATION

Fig. 8 shows that the UAV carries battery packs with a normal voltage of 24 V. We used several battery eliminator circuit (BEC) modules for the buck converter function to convert 24 V to either 12 V or 5 V. However, we used a power over ethernet (PoE) injector for the boost converter function to convert 12 V to 24 V.

C. MECHANICAL SYSTEM CONFIGURATION

The mechanical configuration of the octocopter multi-copter type was based on an environmental monitoring UAV,

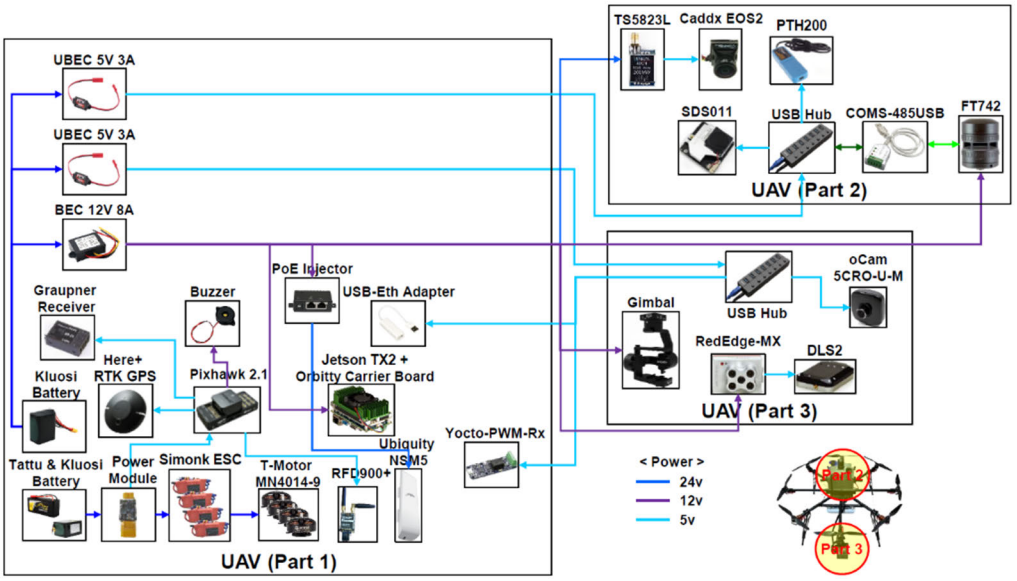

FIGURE 8. Electrical system configuration of the UAV.

TABLE 3. Specification of UAV Mechanical System.

	Detail
Type	Octocopter Radial
Dimension	1140 mm × 1140 mm × 710 mm (W × L × H, motor center to center) 1550 × 1550 × 710 mm (W × L × H, propeller tip to tip)
Weight	13.07 kg (w/ frame, sensors, and batteries) 8.73 kg (w/ frame and sensors)
Sensor	FT 742 Wind Sensor PTH200 Temperature, Humidity, Pressure Sensor SDS011 Air Quality Sensor RedEdge-MX Multispectral Camera oCam RGB Camera Caddx Turbo EOS2 RGB Camera
GPS	Here+ RTK GPS
FC	Pixhawk 2.1 Cube
MC	NVIDIA Jetson TX2 w/ Orbitty Carrier
Max Speed	20 km/h
Radio Range	40 km (without obstacles)
Wi-Fi Range	15 km (without obstacles)
ROS Support	Yes

because of its stable flight performance, to maximize noise-free sensor measurements. Figs. 9 and 10 show the detailed UAV appearance with accompanying sensors and Table 3 lists its specifications.

Tables 4 – 6 list the specifications of the battery pack. We used battery packs #1 and #2 for the UAV thrust and #3 for the sensors.

D. SOFTWARE CONFIGURATION

To maneuver the directional angle of both the multispectral camera and RGB camera mounted on the gimbal, we controlled the yaw angle of the UAV and pitch angle of the gimbal based on the ROS, which was installed on an MC communicating with an FC. We used the micro air vehicle link (MAVLink) communication protocol-based ROS (MAVROS) package, which contains communication

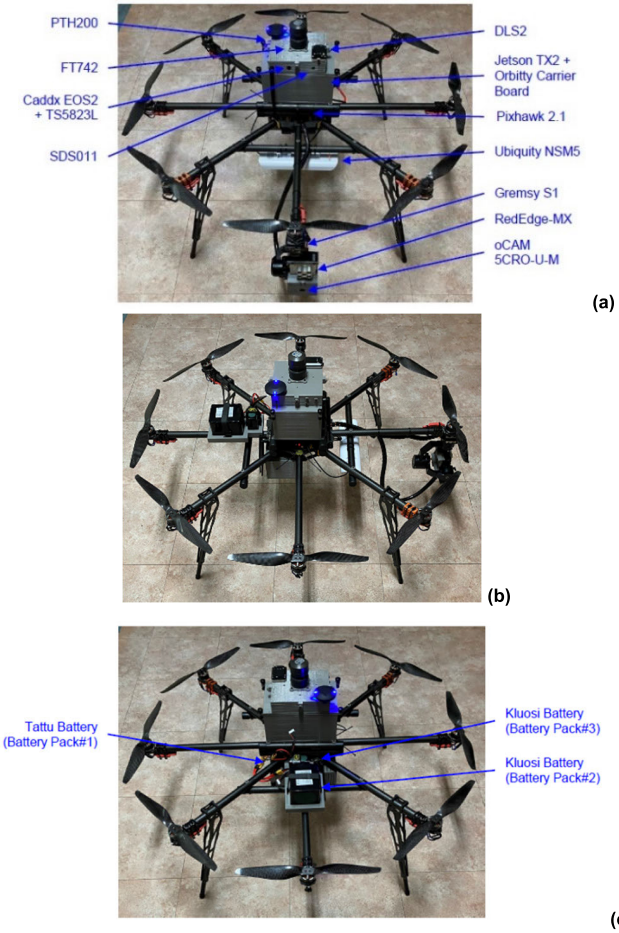

FIGURE 9. Mechanical system configuration of UAV. (a) Front view, (b) rear view, and (c) side view.

FIGURE 10. Details of UAV's mechanical system.

TABLE 4. Specification of Battery Pack #1 in UAV.

	Detail
Type	Tattu Li-Po 6S1P
Dimension	213 mm × 96 mm × 69 mm (L × W × H)
Weight	2.65 kg
Nominal Capacity	22.0 Ah
Nominal Voltage	22.2 V
Nominal Power	488.4 Wh
Constant Discharge	550 A (25 C, 12.21 kW, < 144 s)
Full Discharge	1100 A (50 C, 24.42 kW, < 72 s)
Charging Time	2 h (0.5 C)

TABLE 5. Specification of Battery Pack #2 in UAV.

	Detail
Type	Kluosi Li-Ion 6S5P
Dimension	110 mm × 95 mm × 70 mm (L × W × H)
Weight	1.40 kg
Nominal Capacity	17.5 Ah
Nominal Voltage	22.2 V
Nominal Power	388.5 Wh
Constant Discharge	35 A (2 C, 0.78 kW, < 1800 s)
Full Discharge	105 A (6 C, 2.33 kW, < 600 s)
Charging Time	2 h (0.5 C)

TABLE 6. Specification of Battery Pack #3 in UAV.

	Detail
Type	Kluosi Li-Ion 6S1P
Dimension	38 mm × 55 mm × 70 mm (L × W × H)
Weight	0.29 kg
Nominal Capacity	3.5 Ah
Nominal Voltage	22.2 V
Nominal Power	77.7 Wh
Constant Discharge	7 A (2 C, 0.16 kW, < 1800 s)
Full Discharge	21 A (6 C, 0.47 kW, < 600 s)
Charging Time	2 h (0.5 C)

drivers, for communication among various autopilots using the MAVLink communication protocol. Alternatively, we could use the MAVROS to set the user datagram protocol (UDP) MAVLink bridge between the UAV FC and GCS.

Specifically, we used the desired yaw angle of the UAV, calculated using Pysolar Python libraries [50], to manipulate the bearing of the UAV by overlapping the yaw angle of the waypoint_node, as shown in Fig. 11.

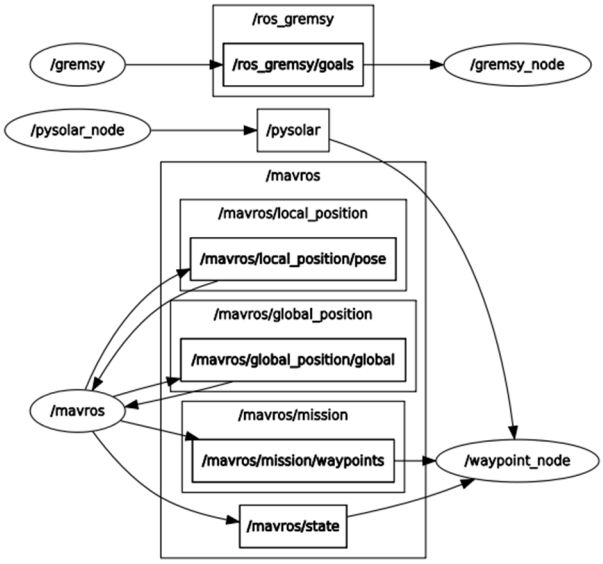

FIGURE 11. SW configuration of the UAV.

We used the Pysolar Python libraries to calculate the azimuth angle:

$$\theta_p = \theta_a - \frac{\pi}{2} \tag{2}$$

Here, the angle of the Pysolar vector (θ_p) was measured from the east (Fig. 12).

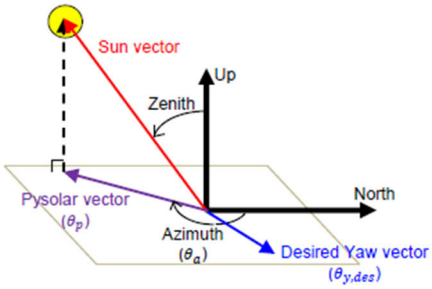

FIGURE 12. Illustration of calculation of the desired yaw vector to which the UAV headed using the solar azimuth.

As seen from Table 7, the UAV used Python-based SW running on the Ubuntu OS.

TABLE 7. Specification of the UAV SW.

	Detail
OS	Ubuntu 16.04 LTS
SW	Python 2.7.12

E. COST ANALYSIS

The required cost to develop the UAV is given from the bill of materials (BOM), listed in Table 8.

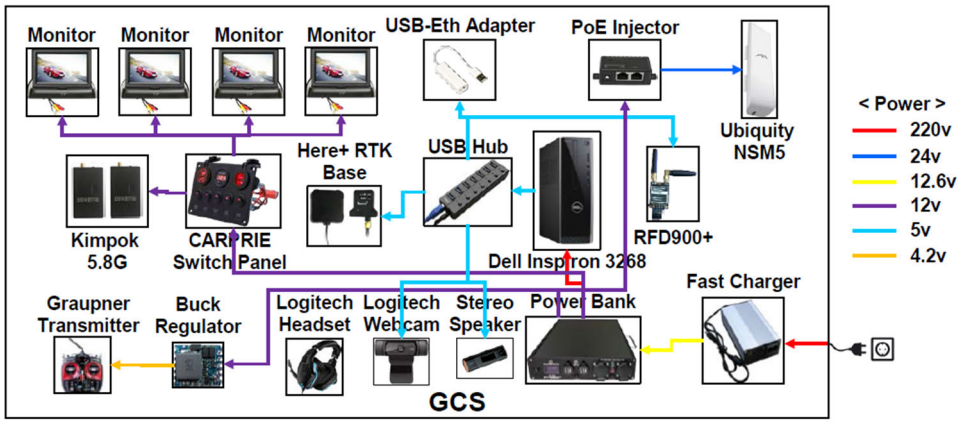

FIGURE 13. Electrical system configuration of the GCS.

TABLE 8. Bill of Materials of the UAV.

	Part	Quantity	Price
UAV (Part 1)	Pixhawk 2.1 Standard Set	1	$290
	Here2 GNSS GPS	1	$120
	Graupner Receiver	1	$60
	Simonk ESC	8	$320
	T-Motor	8	$775
	RFD900+	1	$115
	Jetson TX2	1	$395
	Orbitty Carrier Board	1	$175
	PoE Injector	1	$5
	USB-Eth Adapter	1	$5
	Ubiquity NSM5	1	$90
	Tattu Battery Pack	1	$470
	Kluosi Battery Pack 1	1	$75
	Kluosi Battery Pack 2	1	$20
	BEC 12V 8A	1	$15
	BEC 5V 3A	2	$5
	Yocto-PWM-Rx	1	$65
	UAV Frame & Motor Mount	1	$225
	Propeller	8	$60
	3D Printed Parts	1	$100
UAV (Part 2)	TS5823L	1	$10
	Caddx EOS2	1	$15
	PTH200	1	$130
	SDS011	1	$15
	FT742	1	$2000
	USB Hub	1	$50
	COMS-485USB	1	$30
UAV (Part 3)	Gimbal	1	$1930
	RedEdge-MX Set	1	$6060
	oCam 5CRO-U-M	1	$60
	USB Hub	1	$50
Total		$13 735	

V. GROUND CONTROL STATION

A. SYSTEM REQUIREMENTS

The GCS simultaneously maneuvered the UAV and served as an intermediate medium among the UAV, operator, and server, sending and receiving sensor data in real-time. The main functions of GCS are summarized as follows:

- Communicate with the UAV based on QGC through the MAVLink protocol.
- Have a user-intuitive GUI enabling the GCS operator to start or terminate the automatic UAV flight and sensor measurement operations.
- Receive an analog video (AV) stream from the UAV for stable video communication with low latency.
- Carry a Here+ RTK base GPS module and a Here+ RTK base antenna for centimeter-level global navigation satellite system positioning of the UAV.
- Carry a webcam and headphones with a microphone to allow the GCS operator to communicate with users looking at the web-based data viewer on the website while the UAV is in operation.
- Carry a stereo speaker to amplify the QGC audio output for outdoor usage.

B. ELECTRICAL SYSTEM CONFIGURATION

We installed four 14-in monitors for operator convenience. For stable Wi-Fi communication within a straight-line distance of 15 km, we installed a Ubiquity Nanostation NSM5 to provide a robust Wi-Fi communication connection between the UAV and GCS. As presented in Table 9, we installed a 15 Ah power bank that simultaneously supplied 12 V and 220 V power to achieve a long operation time. We installed a CARPRIE switch panel to serve as the power switch of the monitors and Kimpok AV receivers. The power switches of the desktop PC and power bank were installed in a separate

TABLE 9. Specification of the Power Bank in GCS.

	Detail
Type	Samsung INR18650-29E 2850 mAh 3S54P
Dimension	330 × 550 × 78 mm (W×L×H)
Weight	15 kg
Nominal Capacity	155 Ah
Nominal Voltage	11.1 V
Nominal Power	1720 Wh
Full Discharge	Port1: 10 A, Port2: 6 A, Port3: 220 V w/1000 W
Constant Discharge	Port1: 8 A, Port2: 5 A, Port3: 220 V w/ 1000 W
Charging Time	5 h

area to avoid power cuts because of possible misinterpretation of directions by a non-professional operator. Fig. 13 provides a detailed description of the configuration of the remaining electrical system.

C. MECHANICAL SYSTEM CONFIGURATION

We designed the GCS to be compact, light, and sufficiently portable for a single user, as shown in Fig. 14 and 15. We equipped the exterior with a waterproof function for extreme environments and long indoor and outdoor storage. We designed the GCS interior so that it would be easily attachable and detachable for frequent performance upgrades and maintenance.

Table 9 and 10 provides detailed specifications of the GCS mechanical system.

TABLE 10. Specification of the Mechanical System in GCS.

	Detail
Dimension	820 × 470 × 300 mm (W×L×H, when folded)
Weight	30 kg
Max Operating Time	24 h
CPU	Intel Core i3-7100 Dual-Core 3.9 GHz
Memory	DDR4 32 GB
HDD	1 TB 7200 rpm SATA III Hard Drive

D. SOFTWARE CONFIGURATION

The desktop PC ran Python, QGC, and Qt, as listed in Table 11. We developed a user-intuitive GUI for UAV maneuver and sensor measurement data analysis, as shown in Fig. 16.

TABLE 11. Specification of the GCS SW.

	Detail
OS	Ubuntu 16.04 LTS
SW	Python 2.7.12, QGC v4.0.10, Qt v5.12.6

E. COST ANALYSIS

Table 12 presents the BOM to show the cost required to develop the GCS.

VI. SERVER

A. SYSTEM REQUIREMENTS

A server can be installed anywhere on the Internet. In this study, we placed our server in a university laboratory with a network switch. Because of the university's Internet firewall policy, we needed a network switch to identify the connected server and forward data to the port connected to the server with an assigned media access control (MAC) address. The university information security team constantly monitored the MAC address to prevent hacking attacks. External users who did not have access to the university Internet had to use the assigned MAC address with a secure password to connect to the server and retrieve the sensor measurement dataset.

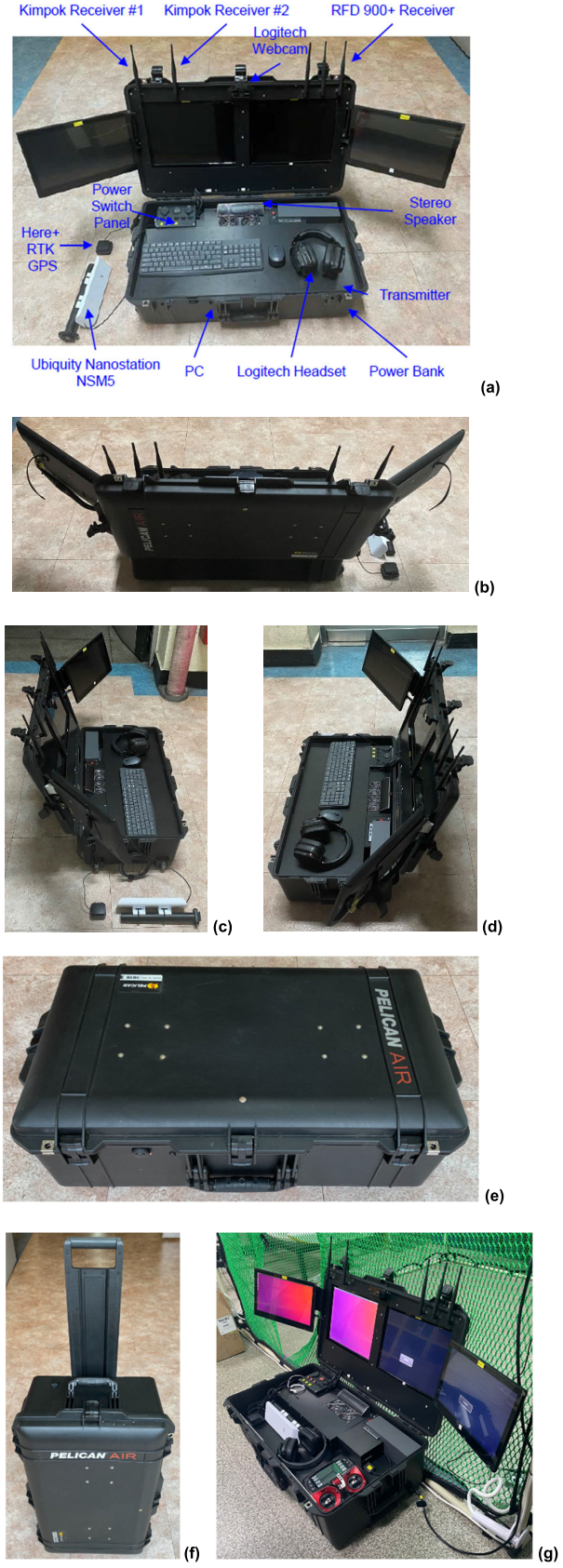

FIGURE 14. Mechanical system configuration of GCS. (a) Front view, (b) rear view, (c) left view, (d) right view, (e) folded view, (f) mobile view, and (g) charging view.

FIGURE 15. Mechanical system details of GCS.

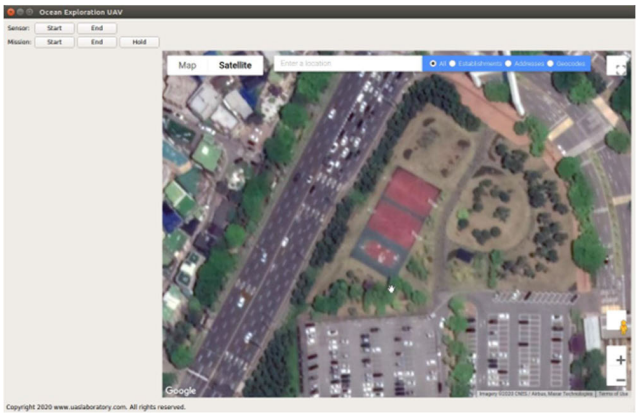

FIGURE 16. GCS GUI.

TABLE 12. Bill of Materials of the GCS.

Part	Quantity	Price
Pelican Air Case	1	$480
Dell Inspiron 3268	1	$600
Power Bank	1	$1790
Fast Charger	1	$310
USB Hub	1	$50
RFD900+	1	$115
PoE Injector	1	$5
Ubiquity NSM5	1	$90
USB-Eth Adapter	1	$5
Here+ RTK Base	1	$610
Carprie Switch Panel	1	$25
Kimpok 5.8G	2	$200
Monitor	4	$540
Buck Regulator	1	$5
Graupner Transmitter	1	$440
Logitech Headset	1	$200
Logitech Webcam	1	$120
Stereo Speaker	1	$30
Total	$5615	

B. ELECTRICAL SYSTEM CONFIGURATION

The network switch connection was the only special connection, as shown in Fig. 17. A customized server PC was wired through an Ethernet line with a network switch.

C. MECHANICAL SYSTEM CONFIGURATION

For robust server management, we installed a customized server PC with high computing power in the laboratory at

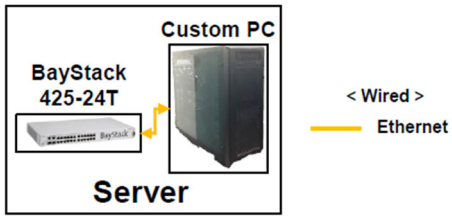

FIGURE 17. Electrical system configuration of the server.

Chosun University, as shown in Fig. 18. Table 13 lists the specifications.

FIGURE 18. Mechanical system of the server.

TABLE 13. Specification of the Mechanical System in the Server.

	Detail
CPU	Dual Intel XEON 4116 (2.1 GB)
Memory	DDR4 128 GB
VGA	GeForce RTX 2070 VENTUS 8 GB
Mainboard	ASUS WS C621E SAGE iBORA
SSD	860 EVO 250 GB
HDD	Seagate 2 TB 64M

D. SOFTWARE CONFIGURATION

In addition to Python, no specific SW was required for the server, as shown in Table 14.

TABLE 14. Specification of the Server SW.

	Detail
OS	Ubuntu 16.04 LTS
SW	Python 2.7.12

E. COST ANALYSIS

Table 15 presents the BOM to show the costs required to develop the server.

TABLE 15. Bill of Materials of the GCS.

Part	Quantity	Price
Custom PC	1	$10 000
BayStack 425-24T	1	$410
Total	$10 410	

VII. EXPERIMENT

This section presents the operational scenario and corresponding flight experiment with flight logs and their analysis. The experiment comprised four steps, ranging from an

TABLE 16. Order of the Experiments.

Step	Experiment Classification	Experiment Type	UAV Type	Experiment Location
1	Indoor Experiment	SILS Experiment	Simulated UAV	Laboratory
2	Outdoor Experiment	Pre-Flight Experiment	F450 UAV	Playground
3			Maritime UAV	
4		Real Flight Experiment		Mission Area

TABLE 17. Results of the SILS Experiment Using a Simulated UAV.

		Detail	
Test UAV		Quadrotor UAV simulated in Gazebo	
Experiment Date		2021-03-26 12:37	
Experiment Location		Lat: 35.143364°, Lon: 126.925803°, Alt: 57 m	
UAV Yaw	θ_a	179.54°	
	$\theta_{y,des}$	44.54°	
	$\overline{\theta_y}$	51.91°	
	$\theta_{y,des} - \overline{\theta_y}$	7.37°	
Gimbal Pitch	$\overline{\theta_c}$	Downward: -	Upward: -
	$\lvert 50° - \lvert\overline{\theta_c}\rvert\rvert$	Downward: -	Upward: -

indoor experiment based on a software-in-the-loop simulation (SILS) to an outdoor experiment to convey all the necessary sensors to the mission area, as presented in Table 16. The level of difficulty corresponds to the number of steps.

To compare the flight logs, we applied a similar square-shaped trajectory pattern for each experimental step. We also cloned the entire system for the same version of SW into each FC and MC used for each experimental step. We used the same SW GUI for the indoor and outdoor experiments, except for Gazebo (which we used only for the indoor experiment), as shown in Fig. 19.

In Tables 17 to 20, θ_a is the real-time solar azimuth angle, calculated by referring to Hoffmann's "SunCalc" [51], $\theta_{y,des}$ is the desired yaw angle of the UAV, θ_y is the yaw angle of the UAV, and θ_c is the pitch angle of the gimbal. In addition, we present the exact experiment date, time, and location because the data are used to calculate the real-time solar azimuth angle θ_a. Specifically, we need to pay attention to using the exact latitude and longitude GPS data by considering the offset between the real location and the location based on the induced GPS data. If the offset is too large, it will affect the home position and can lead the UAV to land at an undesired location after the mission.

A. SILS EXPERIMENT (SIMULATED UAV)

We performed an indoor experiment based on SILS. In the Gazebo SW environment, we used a simulated UAV to determine the proper yawing control functionality based on the solar azimuth angle before the actual UAV flight, as shown in Fig. 20. Table 17 details the experimental data.

B. PRE-FLIGHT EXPERIMENT (F450 UAV)

We performed an outdoor pre-flight experiment on an F450 UAV carrying only a Jetson TX2, assembled with an

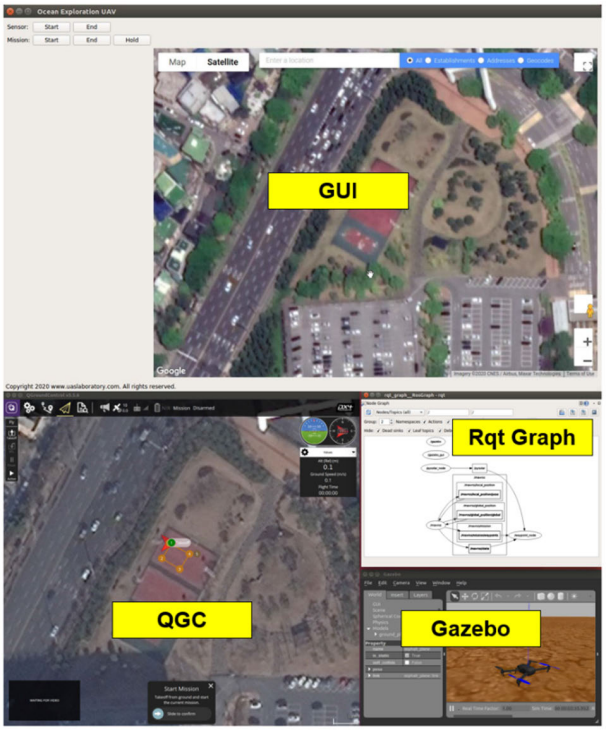

(a)

(b)

FIGURE 19. Experiment setup. (a) SW setup, and (b) HW setup.

TABLE 18. Results of the Pre-Flight Experiment Using an F450 UAV.

		Detail	
Test UAV		F450 quadrotor UAV carrying a Jetson TX2 assembled with an Orbitty Carrier board	
Experiment Date		2021-04-16 12:47	
Experiment Location		Lat: 35.143364°, Lon: 126.925803°, Alt: 57 m	
UAV Yaw	θ_a	188.62°	
	$\theta_{y,des}$	53.62°	
	$\overline{\theta_y}$	61.53°	
	$\lvert\theta_{y,des} - \overline{\theta_y}\rvert$	7.91°	
Gimbal Pitch	$\overline{\theta_c}$	Downward: -	Upward: -
	$\lvert 50° - \lvert\overline{\theta_c}\rvert\rvert$	Downward: -	Upward: -

Orbitty Carrier board but without a sensor to ensure the proper yawing control functionality based on the solar azimuth angle before actual UAV flight, as shown in Fig. 21. Table 18 provides detailed information on the experiments.

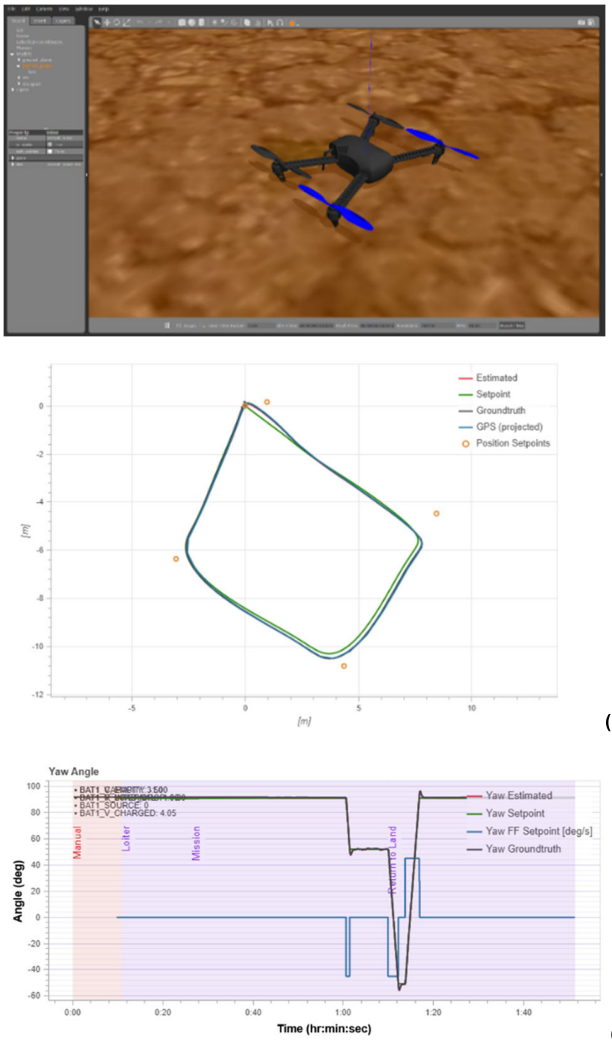

FIGURE 20. Flight log analysis. (a) Simulated UAV used for the SILS experiment, (b) flight trajectory, and (c) yaw angle.

TABLE 19. Results of the Pre-Flight Experiment Using a Maritime UAV.

		Detail	
Test UAV		Maritime octocopter UAV carrying a Jetson TX2 assembled with an Orbitty Carrier board and all environmental sensors	
Experiment Date		2021-04-29 15:02	
Experiment Location		Lat: 35.143364°, Lon: 126.925803°, Alt: 57 m	
UAV Yaw	θ_a	248.67°	
	$\theta_{y,des}$	113.67°	
	$\overline{\theta_y}$	121.61°	
	$\lvert\theta_{y,des} - \overline{\theta_y}\rvert$	7.94°	
Gimbal Pitch	$\overline{\theta_c}$	Downward: 53.56°	Upward: −47.28°
	$\lvert 50° - \lvert\overline{\theta_c}\rvert\rvert$	Downward: 3.56°	Upward: 2.72°

C. PRE-FLIGHT EXPERIMENT (MARITIME UAV)

We performed an outdoor pre-flight experiment on a maritime UAV carrying all sensors to ensure proper functionality of the yawing control based on the solar azimuth angle, the pitching control of the gimbal, and the functionality of the sub-components before the actual UAV flight at the mission area (see Fig. 22). Table 19 provides detailed information on the experiment.

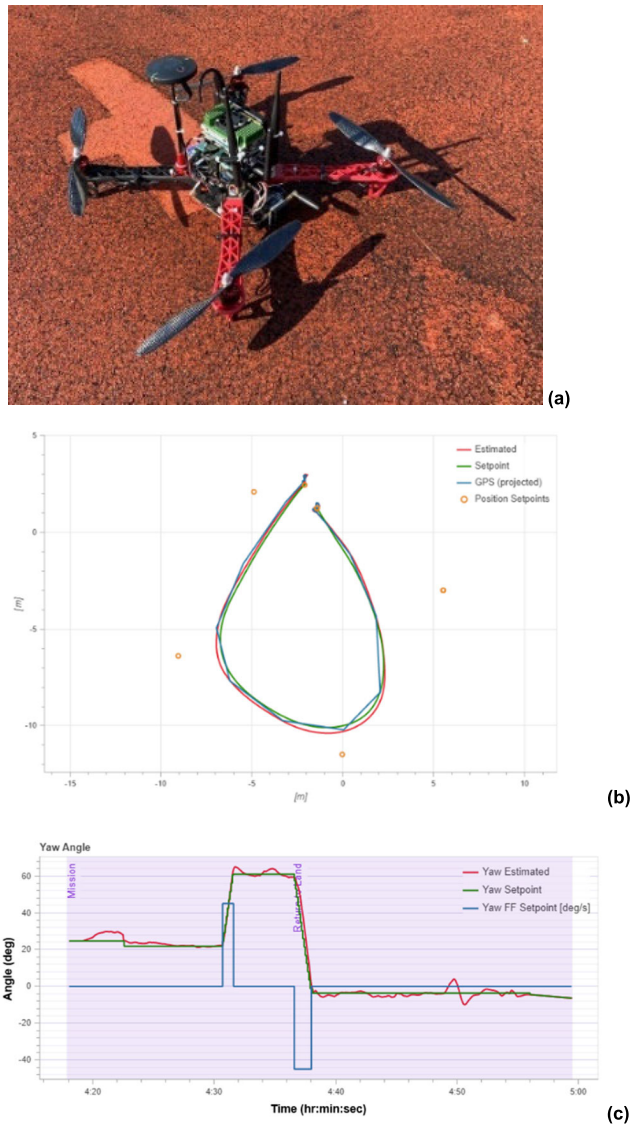

FIGURE 21. Flight log analysis. (a) F450 UAV used for the pre-flight experiment, (b) flight trajectory, and (c) yaw angle.

TABLE 20. Results of the Pre-Flight Experiment Using a Maritime UAV.

		Detail	
Test UAV		Maritime octocopter UAV carrying a Jetson TX2 assembled with an Orbitty Carrier board and all environmental sensors	
Experiment Date		2021-05-06 13:35	
Experiment Location		Lat: 35.004388°, Lon: 126.724007°, Alt: 9 m	
UAV Yaw	θ_a	222.51°	
	$\theta_{y,des}$	87.51°	
	$\overline{\theta_y}$	96.24°	
	$\lvert\theta_{y,des} - \overline{\theta_y}\rvert$	8.73°	
Gimbal Pitch	$\overline{\theta_c}$	Downward: 54.47°	Upward: −47.16°
	$\lvert 50° - \lvert\overline{\theta_c}\rvert\rvert$	Downward: 4.47°	Upward: 2.84°

D. REAL FLIGHT EXPERIMENT (MARITIME UAV)

We performed our final outdoor experiment with a maritime UAV conveying all the sensors to evaluate the functionality of the UAV, as shown in Fig. 23. Table 20 provides detailed information on the experiment.

(a)

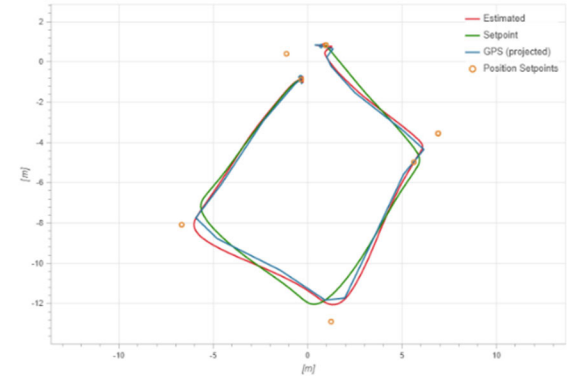

(b)

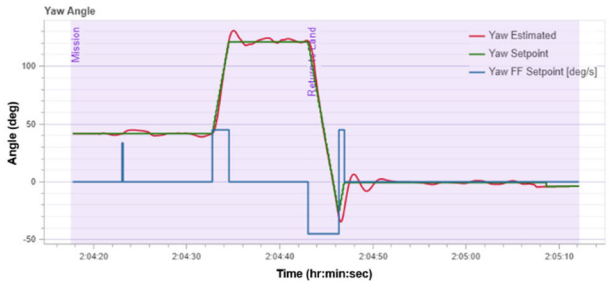

(c)

FIGURE 22. Flight log analysis. (a) Maritime UAV used for the pre-flight experiment, (b) flight trajectory, and (c) yaw angle.

(a)

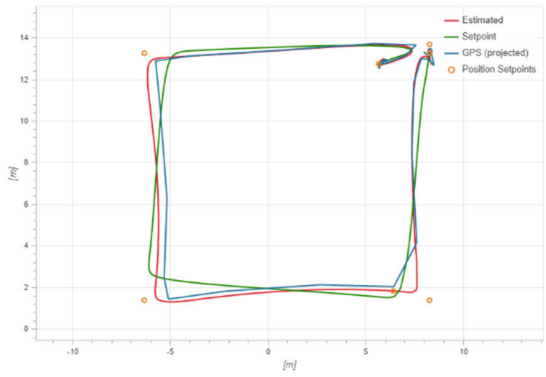

(b)

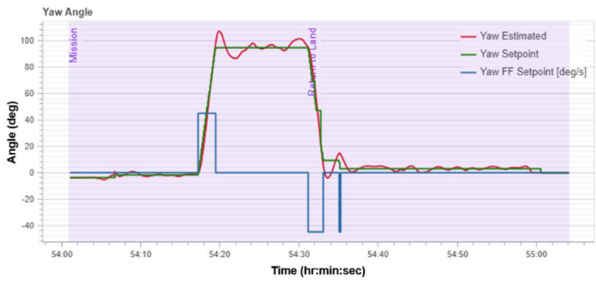

(c)

FIGURE 23. Flight log analysis. (a) Maritime UAV used for the flight experiment, (b) flight trajectory, and (c) yaw angle.

VIII. EXPERIMENT RESULTS

Based on the results of a real flight experiment with a maritime UAV, we verified the following, as shown in Fig. 24.

- Manipulation of the yaw angle of the UAV and pitch angle of the gimbal.
- The sensor data acquisition.

In Fig. 24(a), red represents the heading direction of the UAV, and blue represents the heading direction of the gimbal. It should be noted that both the heading directions of the UAV and the gimbal were well maintained in the pre-assigned direction.

In Fig. 24(b), red indicates the magnitude and directional angle of the wind. As expected, the wind magnitude fluctuates at takeoff and landing because turbulence occurs when the UAV is located near the ground and the generated turbulence disturbs the data measurement of the wind sensor.

From Figs. 24(c) to (g), yellow, green, and blue indicate sensor data including temperature, RH, pressure, PM2.5, and PM10, respectively, depending on the magnitude. If the sensor data magnitude increases, the color becomes yellow, and vice versa.

In Fig. 24(h), purple, orange, yellow, and red represent the UAV trajectory, sun, solar azimuth, and home location, respectively. In addition, white boxes indicate the directions of the north, south, east, and west. Multiple images from the multispectral and RGB cameras were stitched on the ground map. Although not depicted in Fig. 24(h), multiple multispectral and RGB images of the sky were subsequently used to monitor the light conditions at the moment the images were captured.

In Fig. 24(h), we can see that the UAV takeoffs at the home position (red empty circle) and flies along with the predefined waypoints (purple line), while the heading direction of the UAV is 135° away from the solar azimuth (orange circle with white boundary) and finally lands at the preplanned home position again. From the stitched images on the ground

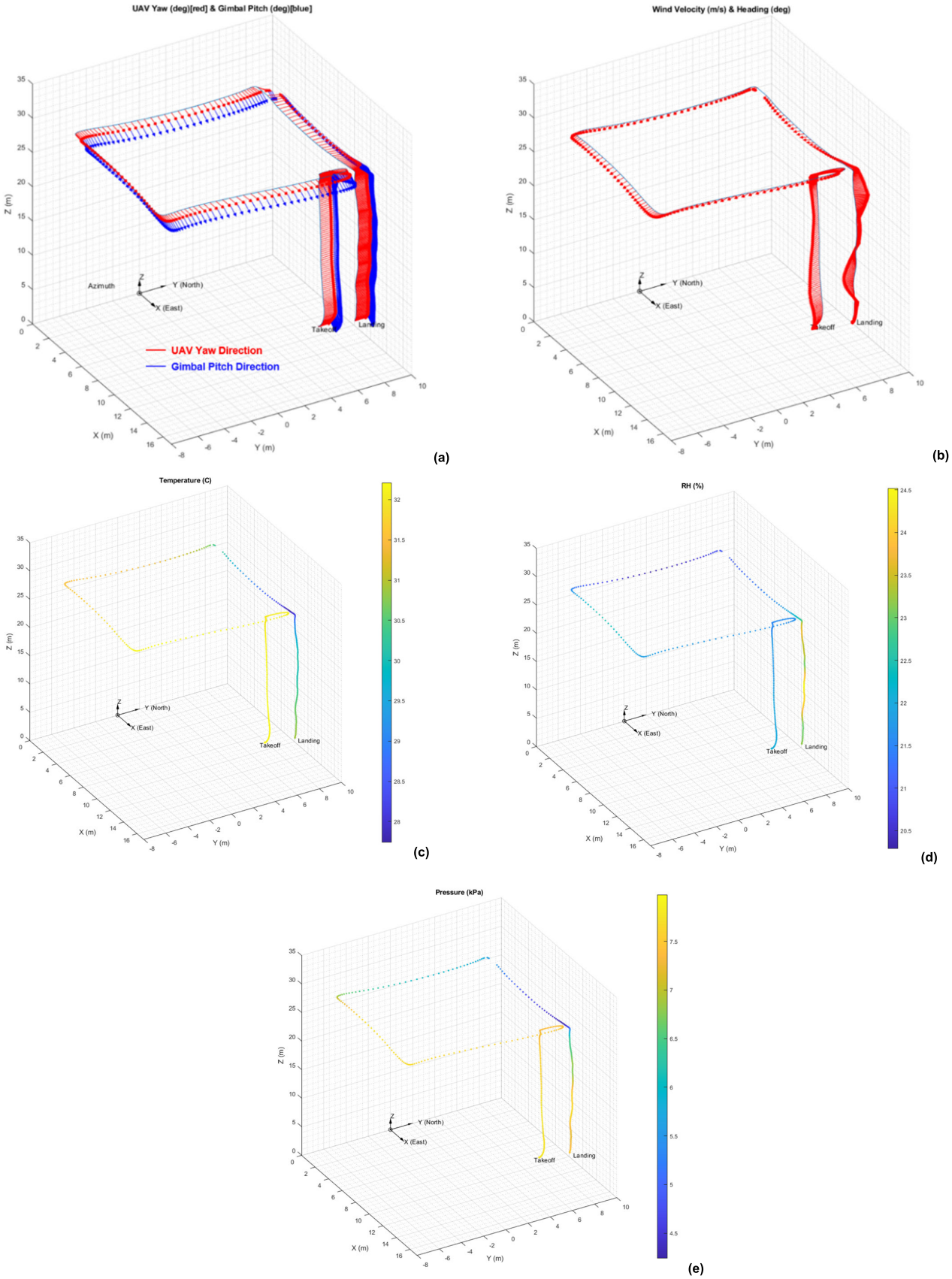

FIGURE 24. Experiment results analysis. (a) Yaw angle of the UAV and pitch angle of the gimbal, (b) wind speed with direction, (c) temperature, (d) RH, (e) pressure, (f) PM2.5, (g) PM10, and (h) multispectral and RGB images.

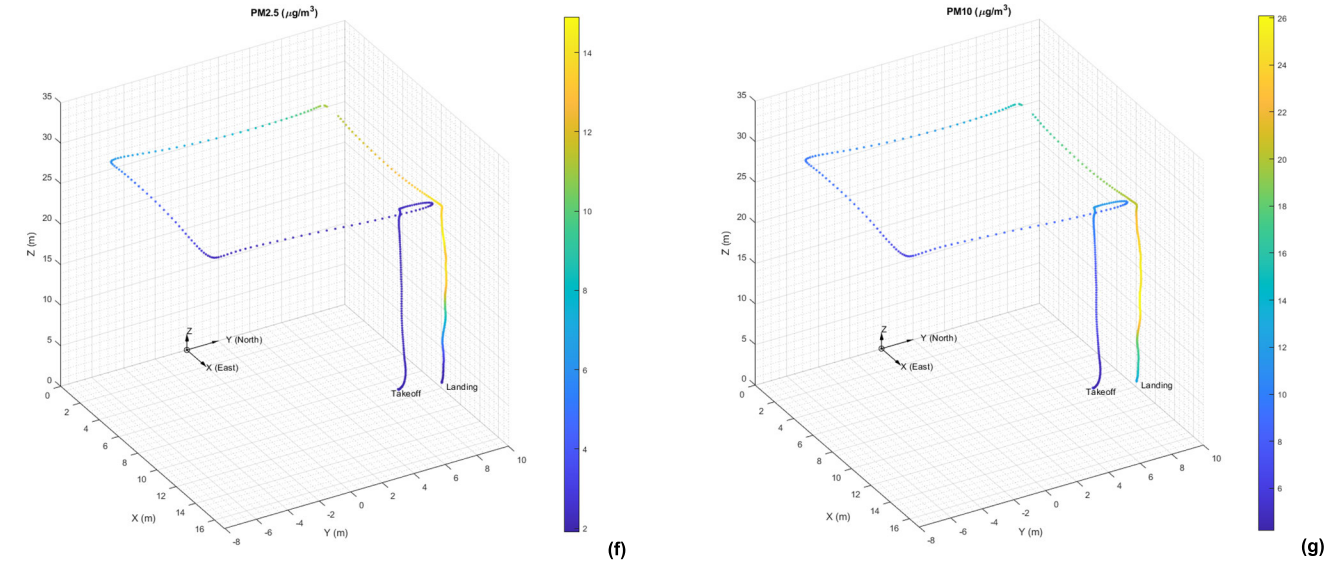

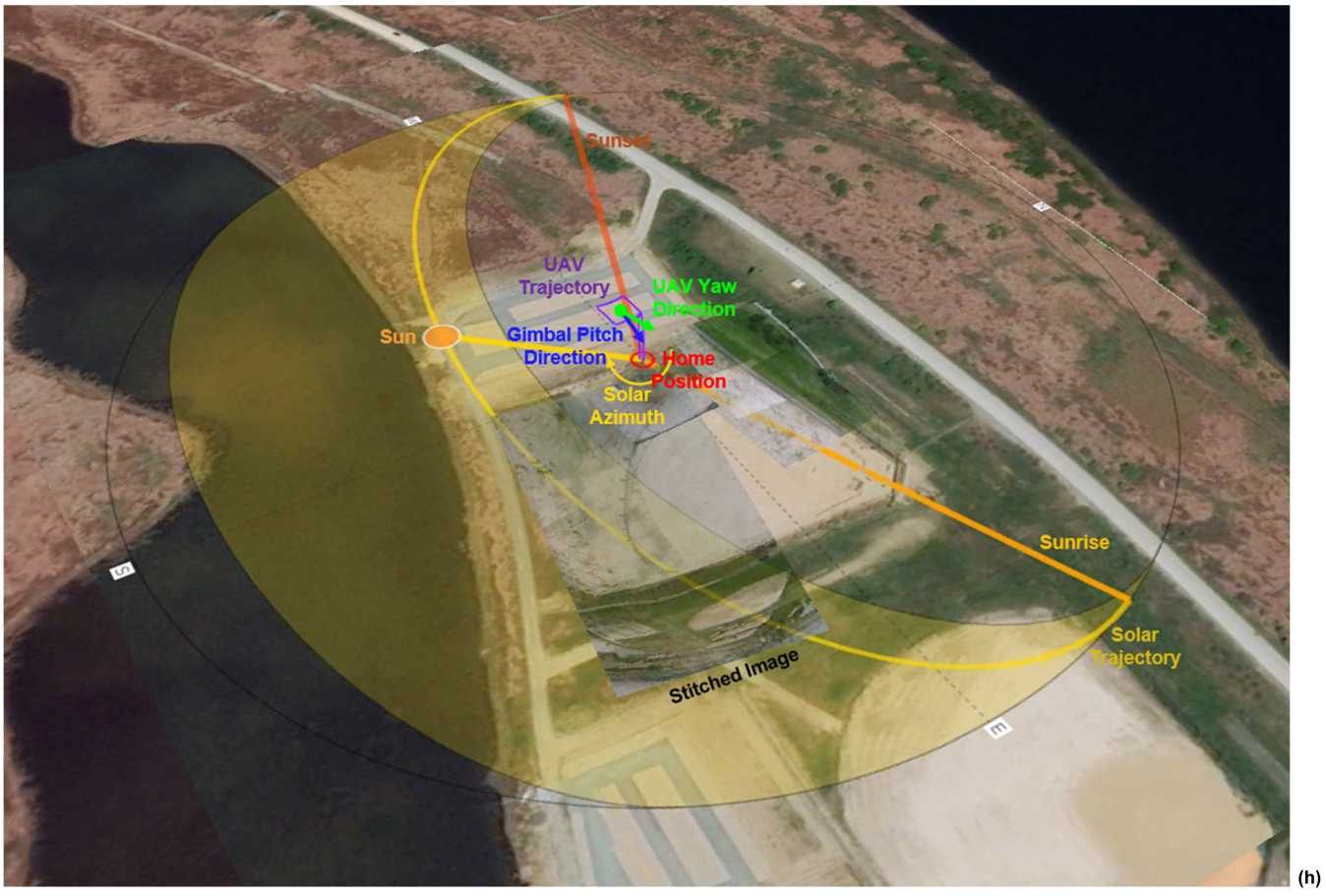

FIGURE 24. *(Continued.)* **Experiment results analysis. (a) Yaw angle of the UAV and pitch angle of the gimbal, (b) wind speed with direction, (c) temperature, (d) RH, (e) pressure, (f) PM2.5, (g) PM10, and (h) multispectral and RGB images.**

in Fig. 24(a), we can conclude that the heading directions of both the UAV and gimbal worked as expected.

We tested a short flight time of approximately 2 min because we only wanted to focus on determining the right attitude control of the UAV and gimbal.

Note that there is no relationship between the average yaw angle error, $\theta_{y,des} - \bar{\theta}_y$, and the experiment times listed in Tables 17 – 20. This is because the desired yaw angle required by the UAV was calculated based on the Pysolar library [50], which was primarily developed to model solar

radiation on Earth. The Pysolar open-source library uses the user's current location, date, and time to calculate solar altitude, azimuth, clear-sky radiation, etc. We considered the weather variable to calculate the solar azimuth angle (the main focus of this study) to control the UAV to back the sun at 135° and thus minimize sunglint on the captured images.

IX. CONCLUSION

In this study, we developed a UAS composed of a UAV, GCS, and a server to measure wind speed and direction, temperature, RH, atmospheric pressure, fine dust, and multispectral and RGB data of the maritime environment. It can control the yaw and gimbal's pitch direction based on the solar incident angle, calculate the amount of reflected light on the captured image, eliminate sun, and, ultimately, estimate seawater constituents.

The main application of the proposed maritime monitoring UAV is to observe ocean color (for example, a red tide), which requires immediate and time-based observations. The MAVROS package controlled the yaw angle of the UAV and the pitch angle of the gimbal, which enabled MAVLink communication among computers running ROS.

Our experimental results indicate that the yaw angle of the maritime UAV maneuvered to 135° from the solar azimuth angle, with the sun at the rear. The average yaw angle error during the mission, $|\theta_{y,des} - \theta_y|$, was approximately 8°. Similarly, the average pitch angle of the gimbal during the mission, $|50° - |\bar{\theta}_c||$, was less than 5°.

With respect to the environmental monitoring sensors, we analyzed the wind speed obtained with direction, temperature, RH, atmospheric pressure, fine dust, and multispectral and RGB data by visualizing 3D graphs along with the UAV trajectory for intuitive analysis.

Although some previous studies yielded relevant results, these have limitations because the experiments were conducted near a reservoir, rather than over an ocean, due to the short flight time that arises from the incapacity of the maritime UAV. In this study, because of concerns about damage arising from a crash into the ocean, we postponed experiments over the ocean area until we could verify the robustness of the system through multiple flight experiments. The short flight time is mostly due to the non-optimized, bulky, and unnecessarily heavy HW and the low energy density of the Li-Po battery pack compared to that of the Li-Ion battery pack. Although we attempted to increase the energy density by hybridizing a 22 Ah Li-Po battery pack, a 17.5 Ah Li-Ion battery pack, and a 3.5 Ah Li-Ion battery pack in this manuscript, we further needed to increase the capacity of the Li-Ion battery pack.

Unfortunately, we did not test the flight time endurance in this project because of fall and breakage risks. To safely test the flight time, our research group is currently designing a three-axis jig-stand system with a three-axis load cell. With this system, we can safely perform an indoor flight endurance test before the actual outdoor flight time endurance system.

The maritime UAV that we developed has an autonomy level between 2 and 3; this is because a pilot needs to activate the UAV with predefined waypoints and activate sensors with predefined measuring time, the UAV automatically flies under limited conditions, etc.

In the future, we expect the maritime UAV to be redesigned to weigh less than 8 kg (with frame, sensors, and batteries); approximately 60% of the weight of the current UAV prototype. This is achieved by replacing the following:

- Octocopter frame with a coaxial quadrotor frame, with smaller motors and propellers.
- Three-axis gimbal with a one-axis gimbal.
- Electric speed controllers (ESCs) with ESCs having a lower maximum permissible current, 3D printed zig (for the internal mounting of sensors) made of polylactic acid material with a zig made of light carbon material.
- Power cables with higher American wire gauge cables.
- USB hubs with a self-made multiple-layered printed circuit board with signal converters for RS-485, Ethernet, USB 2.0, and USB 3.0.

The main purpose of the redesign is to achieve greater stability, maneuverability, and endurance. The flight time of the redesigned maritime UAV is expected to exceed 40 min.

The reason for postponing the flight experiment over the sea area was predominantly due to the unknown flight endurance capability. Notice that the BOM information in Tables 8, 12, and 15 demonstrates an excessively high system cost and we could not ensure the robustness of the UAS for flying over the sea, where a single minor mistake could result in catastrophic mission failure (for example, the loss of the UAV in the seawater). Therefore, we postponed flight tests in proximity to the sea for future work.

In the future, we will mainly focus on reducing the overall UAV weight to less than 8 kg and increasing the flight time to over 40 min. We will also perform thorough robustness tests by focusing mainly on the possibilities and limitations of flight endurance and wind resistance capabilities. We expect to perform dozens of flight tests before initiating the flight experiment over the sea area.

Our primary purpose in publishing this manuscript is to allow remote-sensing researchers, particularly those studying ocean color, and to easily follow up on how to develop an unmanned system-based data acquisition tool. With this in mind, we dedicated ourselves to introducing unmanned system technologies as clearly and as detailed as possible so that non-experience remote-sensing researchers can easily understand it and follow it for their remote-sensing research purposes.

With the systematic information presented in this manuscript, future researchers will be able to develop various types of unmanned systems for maritime data acquisition. We hope that researchers investigating ocean color can reduce their research expenses from direct seawater collection, as well as reduce unexpected human casualties from boarding research vessels in dangerous weather, despite the limitation to coastal seawater.

In a transitional period when unmanned systems are being expanded to various fields of study, particularly remote sensing for the maritime environment, we hope that this manuscript serves as a fundamental reference paper for the development of unmanned remote-sensing systems.

REFERENCES

[1] C. R. McClain, "A decade of satellite ocean color observations," *Annu. Rev. Marine Sci.*, vol. 1, pp. 19–42, Jan. 2009.
[2] S. W. Bailey and P. J. Werdell, "A multi-sensor approach for the on-orbit validation of ocean color satellite data products," *Remote Sens. Environ.*, vol. 102, nos. 1–2, pp. 12–23, May 2006.
[3] J. Wesson, D. Burrage, C. Osburn, V. Maisonet, S. Howden, and X. Chen, "Aircraft and *in situ* salinity and ocean color measurements and comparisons in the Gulf of Mexico," in *Proc. IEEE Int. Geosci. Remote Sens. Symp.*, Jul. 2008, pp. 383–386.
[4] J. Churnside and J. Wilson, "Ocean color inferred from radiometers on low-flying aircraft," *Sensors*, vol. 8, no. 2, pp. 860–876, Feb. 2008.
[5] V. E. Brando, J. L. Lovell, E. A. King, D. Boadle, R. Scott, and T. Schroeder, "The potential of autonomous ship-borne hyperspectral radiometers for the validation of ocean color radiometry data," *Remote Sens.*, vol. 8, no. 150, pp. 1–18, Feb. 2016.
[6] W. Kim, S. Jung, Y. Moon, and S. C. Mangum, "Morphological band registration of multispectral cameras for water quality analysis with unmanned aerial vehicle," *Remote Sens.*, vol. 12, pp. 1–19, Jun. 2020.
[7] A. Klimkowska, I. Lee, and K. Choi, "Possibilities OF UAS for maritime monitoring," *ISPRS-Int. Arch. Photogramm., Remote Sens. Spatial Inf. Sci.*, vol. XLI–B1, pp. 885–891, Jun. 2016.
[8] D. Ventura, A. Bonifazi, M. F. Gravina, A. Belluscio, and G. Ardizzone, "Mapping and classification of ecologically sensitive marine habitats using unmanned aerial vehicle (UAV) imagery and object-based image analysis (OBIA)," *Remote Sens.*, vol. 10, no. 1331, pp. 1–23, Aug. 2018.
[9] T. Lukaczyk, T. Bieri, J. T. de Sousa, J. Levy, and P. A. McGillivary, "Unmanned aircraft as mobile components of ocean observing systems for management of marine resources," in *Proc. OCEANS MSTS/IEEE Monterey*, Sep. 2016, pp. 1–7.
[10] A. P. Colefax, P. A. Butcher, and B. P. Kelaher, "The potential for unmanned aerial vehicles (UAVs) to conduct marine fauna surveys in place of manned aircraft," *ICES J. Mar. Sci.*, vol. 75, no. 1, pp. 1–8, Jan. 2018.
[11] A. Hodgson, N. Kelly, and D. Peel, "Unmanned aerial vehicles (UAVs) for surveying marine fauna: A dugong case study," *PLoS ONE*, vol. 8, no. 11, Nov. 2013, Art. no. e79556.
[12] A. Hodgson, D. Peel, and N. Kelly, "Unmanned aerial vehicles for surveying marine fauna: Assessing detection probability," *Ecol. Appl.*, vol. 27, no. 4, pp. 1253–1267, Apr. 2017.
[13] W. R. Koski, T. Allen, D. Ireland, G. Buck, P. R. Smith, A. M. Macrander, M. A. Halick, C. Rushing, D. J. Sliwa, and T. L. McDonald, "Evaluation of an unmanned airborne system for monitoring marine mammals," *Aquatic Mammals*, vol. 35, no. 3, pp. 347–357, Sep. 2009.
[14] J. Fortuna, F. Ferreira, R. Gomes, S. Ferreira, and J. Sousa, "Using low cost open source UAVs for marine wild life monitoring—Field report," *IFAC Proc. Volumes*, vol. 46, no. 30, pp. 291–295, 2013.
[15] L. Fiori, A. Doshi, E. Martinez, M. B. Orams, and B. Bollard-Breen, "The use of unmanned aerial systems in marine mammal research," *Remote Sens.*, vol. 9, no. 543, pp. 1–13, May 2017.
[16] U. K. Verfuss, A. S. Aniceto, D. V. Harris, D. Gillespie, S. Fielding, G. Jiménez, P. Johnston, R. R. Sinclair, A. Sivertsen, S. A. Solbø, R. Storvold, M. Biuw, and R. Wyatt, "A review of unmanned vehicles for the detection and monitoring of marine fauna," *Mar. Pollut. Bull.*, vol. 140, pp. 17–29, Mar. 2019.
[17] A. P. Colefax, P. A. Butcher, D. E. Pagendam, and B. P. Kelaher, "Reliability of marine faunal detections in drone-based monitoring," *Ocean Coastal Manage.*, vol. 174, pp. 108–115, May 2019.
[18] A. C. Seymour, J. Dale, M. Hammill, P. N. Halpin, and D. W. Johnston, "Automated detection and enumeration of marine wildlife using unmanned aircraft systems (UAS) and thermal imagery," *Sci. Rep.*, vol. 7, no. 1, Mar. 2017, Art. no. 45127.
[19] J. Garcia and J. M. Molina, "Simulation in real conditions of navigation and obstacle avoidance with PX4/Gazebo platform," in *Proc. IEEE Int. Conf. Pervas. Comput. Commun. Workshops*, Mar. 2019, pp. 1–21.
[20] E. Ebeid, M. Skriver, and J. Jin, "A survey on open-source flight control platforms of unmanned aerial vehicle," in *Proc. Euromicro Conf. Digit. Syst. Design (DSD)*, Aug. 2017, pp. 1–7.
[21] J. Jackson, G. Ellingson, and T. McLain, "ROSflight: A lightweight, inexpensive MAV research and development tool," in *Proc. Int. Conf. Unmanned Aircr. Syst. (ICUAS)*, Jun. 2016, pp. 758–762.
[22] X. Chen, S. K. Phang, M. Shan, and B. M. Chen, "System integration of a vision-guided UAV for autonomous landing on moving platform," in *Proc. 12th IEEE Int. Conf. Control Autom. (ICCA)*, Jun. 2016, pp. 761–766.
[23] T. Haus, M. Orsag, A. P. Nunez, S. Bogdan, and D. M. Lofaro, "Centroid vectoring for attitude control of floating base robots: From maritime to aerial applications," *IEEE Access*, vol. 7, pp. 16021–16031, 2019.
[24] A. Segales, R. Gregor, J. Rodas, D. Gregor, and S. Toledo, "Implementation of a low cost UAV for photogrammetry measurement applications," in *Proc. Int. Conf. Unmanned Aircr. Syst. (ICUAS)*, Jun. 2016, pp. 926–932.
[25] J. K. Tharamuttam and A. K. Ng, "Design and development of an automatic solar tracker," *Energy Proc.*, vol. 143, pp. 629–634, Dec. 2017.
[26] M. E. H. Chowdhury, A. Khandakar, B. Hossain, and R. Abouhasera, "A low-cost closed-loop solar tracking system based on the sun position algorithm," *J. Sensors*, vol. 2019, pp. 1–11, Feb. 2019.
[27] C. Jamroen, P. Komkum, S. Kohsri, W. Himananto, S. Panupintu, and S. Unkat, "A low-cost dual-axis solar tracking system based on digital logic design: Design and implementation," *Sustain. Energy Technol. Assessments*, vol. 37, pp. 1–14, Feb. 2020.
[28] S. O'Young and P. Hubbard, "RAVEN: A maritime surveillance project using small UAV," in *Proc. IEEE Conf. Emerg. Technol. Factory Autom. (EFTA)*, Sep. 2007, pp. 904–907.
[29] W. Zang, J. Lin, Y. Wang, and H. Tao, "Investigating small-scale water pollution with UAV remote sensing technology," in *Proc. World Automat. Congr.*, Jun. 2012, pp. 1–4.
[30] D. Cook, P. Strong, S. Garrett, and R. Marshall, "A small unmanned aerial system (UAS) for coastal atmospheric research: Preliminary results from New Zealand," *J. Roy. Soc. New Zealand*, vol. 43, no. 2, pp. 108–115, Jun. 2013.
[31] W. Jo, Y. Hoashi, L. L. P. Aguilar, M. Postigo-Malaga, J. M. Garcia-Bravo, and B. C. Min, "A low-cost and small USV platform for water quality monitoring," *HardwareX*, vol. 6, pp. 1–13, Oct. 2019.
[32] Y. Kaizu, M. Iio, H. Yamada, and N. Noguchi, "Development of unmanned airboat for water-quality mapping," *Biosystems Eng.*, vol. 109, no. 4, pp. 338–347, Aug. 2011.
[33] B. Esakki, S. Ganesan, S. Mathiyazhagan, K. Ramasubramanian, B. Gnanasekaran, and B. Son, "Design of amphibious vehicle for unmanned missions in water quality monitoring using Internet of Things," *Sensors*, vol. 18, no. 3318, pp. 1–23, Oct. 2018.
[34] E. Casella, J. Drechsel, C. Winter, M. Benninghoff, and A. Rovere, "Accuracy of sand beach topography surveying by drones and photogrammetry," *Geo-Marine Lett.*, vol. 40, no. 2, pp. 255–268, Jan. 2020.
[35] L. Y. Sorensen, L. T. Jacobsen, and J. P. Hansen, "Low cost and flexible UAV deployment of sensors," *Sensors*, vol. 17, no. 12, pp. 1–13, Jan. 2017.
[36] A. Papakonstantinou, K. Topouzelis, and M. Doukari, "UAS close range remote sensing for mapping coastal environments," in *Proc. 5th Int. Conf. Remote Sens. Geoinformation Environ. (RSCy)*, Sep. 2017, pp. 1–7.
[37] S. P. Garaba, J. Schulz, M. R. Wernand, and O. Zielinski, "Sunglint detection for unmanned and automated platforms," *Sensors*, vol. 12, no. 9, pp. 12545–12561, Sep. 2012.
[38] S. Wang, L. Liu, L. Qu, C. Yu, Y. Sun, F. Gao, and J. Dong, "Accurate ulva prolifera regions extraction of UAV images with superpixel and CNNs for ocean environment monitoring," *Neurocomputing*, vol. 348, pp. 158–168, Jul. 2019.
[39] G. Goncalves, U. Andriolo, L. Pinto, and F. Bessa, "Mapping marine litter using UAS on a beach-dune system: A multidisciplinary approach," *Sci. The Total Environ.*, vol. 706, pp. 1–41, Mar. 2020.
[40] K. Topouzelis, A. Papakonstantinou, and S. P. Garaba, "Detection of floating plastics from satellite and unmanned aerial systems (Plastic Litter Project 2018)," *Int. J. Appl. Earth Observ. Geoinf.*, vol. 79, pp. 175–183, Jul. 2019.
[41] K. E. Joyce, S. Duce, S. M. Leahy, J. Leon, and S. W. Maier, "Principles and practice of acquiring drone-based image data in marine environments," *Mar. Freshwater Res.*, vol. 70, no. 7, pp. 952–963, Jul. 2018.
[42] M. Doukari, M. Batsaris, A. Papakonstantinou, and K. Topouzelis, "A protocol for aerial survey in coastal areas using UAS," *Remote Sens.*, vol. 11, no. 1913, pp. 1–19, Aug. 2019.

[43] P. C. Gray, J. T. Ridge, S. K. Poulin, A. C. Seymour, A. M. Schwantes, J. J. Swenson, and D. W. Johnston, "Integrating drone imagery into high resolution satellite remote sensing assessment of estuarine environments," *Remote Sens.*, vol. 10, no. 1257, pp. 1–24, Aug. 2018.
[44] S. Manfreda, M. F. McCabe, P. E. Miller, and R. Lucas, "On the use of unmanned aerial system for environmental monitoring," *Remote Sens.*, vol. 10, no. 641, pp. 1–28, Apr. 2018.
[45] M. M. Nowak, K. Dziób, and P. Bogawski, "Unmanned aerial vehicles (UAVs) in environmental biology: A review," *Eur. J. Ecol.*, vol. 4, no. 2, pp. 56–74, Jan. 2019.
[46] D. W. Johnston, "Unoccupied aircraft systems in marine science and conservation," *Annu. Rev. Mar. Sci.*, vol. 11, no. 1, pp. 439–463, Jan. 2019.
[47] W. Kim, S. H. Roh, Y. Moon, and S. Jung, "Evaluation of RedEdge-M camera for water color observation after image preprocessing," *J. Korean Soc. Surv., Geodesy, Photogramm. Cartography*, vol. 37, no. 3, pp. 167–175, Jun. 2019.
[48] C. D. Mobley, "Estimation of the remote-sensing reflectance from above-surface measurements," *Appl. Opt.*, vol. 38, no. 36, pp. 7442–7455, Dec. 1999.
[49] Dronecode. *QGroundControl*. Accessed: Apr. 14, 2021. [Online]. Available: http://qgroundcontrol.com
[50] B. Stafford. *Pysolar: Staring Directly at the Sun Since 2007*. Accessed: Apr. 14, 2021. [Online]. Available: https://bit.ly/3deqdYp
[51] T. Hoffmann. *SunCalc*. Accessed: Apr. 14, 2021. [Online]. Available: https://www.suncalc.org

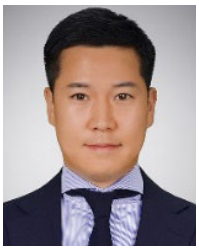

SUNGHUN JUNG (Member IEEE) received the B.S. degree in mechanical engineering from the University of Minnesota Twin Cities, Minneapolis, MN, USA, in 2009, and the M.S. and Ph.D. degrees in mechanical engineering from Purdue University, West Lafayette, IN, USA, in 2010 and 2013, respectively.

From 2014 to 2016, he was a Principal Researcher at Samsung SDI. From 2016 to 2018, he was an Assistant Professor with the Department of Drone System, Chodang University. From 2018 to 2020, he was an Assistant Professor with the Department of Electric Vehicle Engineering, Dongshin University. Since 2020, he has been an Assistant Professor with the Faculty of Smart Vehicle System Engineering, Chosun University, Gwangju, South Korea. His research interests include control and optimization for autonomous operation of unmanned assets, particularly UAVs, energy-efficient path planning using system control and optimization methods, development of state estimation algorithms for battery pack systems, and development of configurable model-based software platforms.

WONKOOK KIM (Member, IEEE) received the Ph.D. degree in civil engineering from Purdue University, West Lafayette, IN, USA, in 2011.

He was a Postdoctoral Researcher on satellite sensor calibration at the Department of Geographical Sciences, University of Maryland, and the National Environmental Satellite, Data, and Information Service (NESDIS), National Oceanic and Atmospheric Administration (NOAA), College Park, MD, USA. From 2013 to 2019, he was a Senior Researcher at Korea Ocean Satellite Research Center, Korea Institute of Ocean Science and Technology, South Korea, where he undertook Cal/Val and algorithm development for ocean color satellites. He is currently an Assistant Professor at the Department of Civil and Environmental Engineering, Pusan National University, South Korea. His research interests include calibration and validation of satellite sensors, development of geophysical retrieval algorithms, and application of machine learning techniques for remote-sensing data.